Calculation of spin-dependent momentum distributions in iron: Compton scattering and positron annihilation



1991 J. Phys.: Condens. Matter 3 1113

(http://iopscience.iop.org/0953-8984/3/9/008)

J. Phys.: Condens. Matter 3 (1991) 1113–1131. Printed in the UK

# Calculation of spin-dependent momentum distributions in iron: Compton scattering and positron annihilation

V Sundararajan†, D G Kanhere† and R M Singru‡

† Department of Physics, University of Poona, Pune 411007, India

‡ Department of Physics, Indian Institute of Technology, Kanpur 208016, India

Received 31 May 1990, in final form 20 November 1990

**Abstract.** Spin-dependent momentum distributions in ferromagnetic iron are calculated in detail using the linear combination of Gaussian orbitals method. Theoretical results for Compton scattering and positron annihilation are presented in the form of momentum distributions, Compton profiles, one-dimensional angular correlation of annihilation radiation curves, Lock–Crisp–West folded plots and reciprocal form factors $B(z)$, and are compared with experiment wherever possible. It is observed that the present theoretical results show satisfactory agreement with experiment. It is further observed that although the different theories (e.g. augmented plane waves, linear muffin-tin orbitals, present linear combination of Gaussian orbitals) agree among each other about the spin-dependent momentum distributions in ferromagnetic iron, minor differences exist between these theories and experiment. These differences are ascribed to the limitations of the independent-particle approximation, in particular to the effects of non-locality, $e^-$–$e^-$ and $e^+$–$e^-$ many-body correlations, etc.

## 1. Introduction

It has been well recognized that the band structures and Fermi surface (FS) properties of iron are of great interest because of their complex nature [1] and because iron exhibits ferromagnetism below 1043 K. In spite of several theoretical and experimental studies, certain ambiguity still exists about the FS topology of iron [2]. Thus, for example, experiments using the de Haas–van Alphen effect [3, 4] and magnetoresistance oscillations [5, 6] have provided results that are not yet completely reconciled with theory. Recently the techniques of measurement of Compton profiles (CP) [7] and angular correlation of (positron) annihilation radiation (ACAR) [8–11] have shown that these studies of momentum distributions (MD) can lead us to a better understanding of the FS topology in metals. Various studies of the CP and ACAR for different transition metals have supported the conclusion that different band-structure methods in the independent-particle model (IPM) can provide a sound theoretical basis to compare theory with experiment [7–11] and that the many-body correlation ($e^-$–$e^-$ or $e^-$–$e^+$) corrections can be added on to the IPM theory. Another special advantage available with the CP and ACAR techniques for the study of iron is that they are capable of measuring effects of spin-dependent (i.e. majority- and minority-spin electrons) MD using either circularly polarized radiation (for CP) or longitudinally polarized positrons (for ACAR). Such experimental studies of spin-dependent CP [12–16] and ACAR [17–20] have provided

0953-8984/91/091113 + 19 $03.50 

valuable information about the spin-dependent wavefunctions of band electrons in ferromagnetic iron. On the theoretical side, calculations of the MD in iron using Hubbard's approximate scheme [18], augmented plane-wave (APW) [21–23], Korringa–Kohn–Rostoker (KKR) [24, 25], linear combination of Gaussian orbitals (LCGO) [26], generalized $k \cdot p$ interpolation scheme [27] and linear muffin-tin orbitals (LMTO) [20, 28] methods have shown that the spin-dependent MD in iron is very sensitive to its FS topology.

Among the different band-structure methods used for the calculation of MD, the *LCGO method* [29, 30] carries certain special advantages such as (i) its self-consistent (SC) character, (ii) the absence of any shape-dependent approximations and (iii) the Gaussian nature of the basis functions and hence its ability to compute the MD up to a desired high momentum ($p$) value analytically (and without much loss of accuracy). The last advantage is especially important in making a realistic comparison between experiment and theory because the theoretical computations involve the integration of the MD over one (or two) components of the momentum (see equations (3), (6) and (7) in section 2 later) and hence the accuracy of the theoretical curves (CP or ACAR) is limited by the knowledge of band MD at high momenta. This is particularly important for the case of iron where the spin-dependent CP are observed to extend up to $p = 8.0$ au [16]. While the MD calculated by the APW method, for example, usually extends up to $p = 5$–$7$ au only, the LCGO method allows a calculation of MD up to (or beyond) $p = 10$ au [31]. Although the LCGO method has been used earlier for the calculation of MD relevant for the CP results for iron [26], we present here a more comprehensive calculation of the MD in ferromagnetic iron incorporating the following two refinements of the earlier work [26]:

(i) We have improved the description of the exchange–correlation (XC) potential. A previous calculation by Rath *et al* [26] used the exchange-only approximation, while that by Callaway and Wang [30] used the spin-polarized exchange potential of von Barth and Hedin [32]. However, in the work of Callaway and Wang [30], the emphasis was on the study of the effect of different crystal potentials on different electronic properties of iron, and the spin-dependent CP was reported only for a polycrystalline sample while the details of the MD, directional CP, etc., were not presented. These details of the MD and directional CP, and their dependence on FS topology, are discussed here in greater detail. To ensure a better description of the correlation effects, we have used the exchange–correlation potential of von Barth and Hedin [32] as parametrized by Rajagopal *et al* [33].

(ii) We have recently extended [31, 34, 35] the LCGO method to perform the calculation of the two-photon momentum distribution (TPMD), which is the physical quantity of central interest in the ACAR studies. In this way we could use the same band-structure method and the same set of electron wavefunctions to calculate the electron momentum distribution (EMD) and TPMD to facilitate a better comparison between theory and experiment (CP and ACAR).

Our application of this refined version of the LCGO method to V [31], Cr [31], Ni [31] and Cu [34, 35] has already provided a satisfactory theoretical description of the experimental results obtained by the CP and ACAR studies. We therefore found it interesting to apply the refined LCGO method for the calculation of spin-dependent EMD and TPMD in ferromagnetic iron. Such a calculation has ensured that the *same* band-structure method and the *same* set of electronic wavefunctions are used to calculate the

theoretical CP and ACAR curves, which can then be compared with the appropriate experiment.

The present paper describes our theoretical results for the calculation of the EMD, $\rho(\boldsymbol{p})$, and the TPMD, $\rho^{2\gamma}(\boldsymbol{p})$, for the majority- and minority-spin electrons of ferromagnetic iron. The results for these MD are shown in the form of two-dimensional (2D) surfaces as well as contour plots to bring out the effects of FS topology. The CP, one-dimensional (1D) and 2D ACAR curves are also computed from these MD and they are compared with the experimental data wherever available. The plots of the MD folded by using the so-called Lock–Crisp–West (LCW) theorem [36] are also presented. The autocorrelation functions (or the reciprocal form factors) $B(z)$ [7, 8] have also been calculated for the CP and ACAR cases and are compared among each other and with experiment. In this way we have tried to present a fairly comprehensive report on the MD in ferromagnetic iron. We believe that the present LCGO-based results would be useful in assessing the local density approximation and neglect of electron–positron correlation by providing an IPM theory that can be carefully compared with experimental data.

The plan of the present paper is as follows. The calculational procedure used by us is outlined in section 2. The results of the present calculations are given in section 3 along with a comparison with experiment wherever possible. In particular, the present theoretical results for the FS, MD, CP (non-magnetic and magnetic) and ACAR along with the plots for LCW-folded distribution and autocorrelation function $B(z)$ are given. These results are discussed in terms of the FS and other properties of iron. Finally a summary is presented in section 4.

## 2. Calculational procedure

*In this section we shall outline our computational procedure briefly. The details of this* procedure are described elsewhere [29, 31, 34, 35]. The EMD is defined as

$$\rho(\boldsymbol{p}) = \sum_{n,k}^{\text{occ}} |\Psi_n(\boldsymbol{k}, \boldsymbol{p})|^2 \tag{1}$$

where $\Psi_n(\boldsymbol{k}, \boldsymbol{p})$ is the momentum-space wavefunction for an electron in a state specified by band index $n$ and wavevector $\boldsymbol{k}$ and is related to the position-space wavefunction $\Psi_n(\boldsymbol{k}, \boldsymbol{r})$ via the Dirac transforms

$$\Psi_n(\boldsymbol{k}, \boldsymbol{p}) = (N\Omega)^{-1/2} \int \exp(-\mathrm{i}\boldsymbol{p} \cdot \boldsymbol{r}) \Psi_n(\boldsymbol{k}, \boldsymbol{r})\, \mathrm{d}\boldsymbol{r} \tag{2}$$

where $\Omega$ is the volume of the unit cell. The CP along the direction $\boldsymbol{p}$ is defined as

$$J_{\hat{k}}(q) = [\Omega/(2\pi)^3] \int \mathrm{d}\boldsymbol{p}\, \rho(\boldsymbol{p}) \delta(q - \boldsymbol{p} \cdot \hat{k}) \tag{3}$$

where

$$q = mw/(|\boldsymbol{k}| - \tfrac{1}{2}|\boldsymbol{k}|) \qquad \text{and} \qquad \hat{k} = \boldsymbol{k}/|\boldsymbol{k}|.$$

The TPMD is defined as

$$\rho^{2\gamma}(\boldsymbol{p}) = \text{const} \sum_{n,k}^{\text{occ}} |F_k^n(\boldsymbol{p})|^2 \delta(\boldsymbol{p} - \boldsymbol{k} - \boldsymbol{G}) \tag{4}$$

where $F_k^n(\boldsymbol{p})$ is the electron–positron overlap integral written as

$$F_k^n = \int_{\text{crystal}} \exp(-i\boldsymbol{p}\cdot\boldsymbol{r})\Psi_+(\boldsymbol{r})\Psi_n(\boldsymbol{k},\boldsymbol{r})\,d\boldsymbol{r} \tag{5}$$

with $\Psi_+(\boldsymbol{r})$ being the positron wavefunction for the lowest-energy state $\boldsymbol{k}_+ = 0$. The 1D ACAR curve in the direction of $\hat{k}$ is given by

$$N_{\hat{k}}(q) = \int d\boldsymbol{p}\, \rho^{2\gamma}(\boldsymbol{p})\delta(q - \boldsymbol{p}\cdot\hat{\boldsymbol{k}}) \tag{6}$$

while the 2D ACAR curves are defined by

$$N(p_y, p_z) = \int_{-\infty}^{+\infty} \rho^{2\gamma}(\boldsymbol{p})\,dp_x. \tag{7}$$

In the LCGO method, the electron and positron wavefunctions are written as

$$\Psi_n(\boldsymbol{k},\boldsymbol{r}) = \sum_j C_{nj}(\boldsymbol{k})\varphi_j(\boldsymbol{k},\boldsymbol{r}) \tag{8}$$

and

$$\Psi_+(\boldsymbol{r}) = \sum_j C_j(\boldsymbol{k}_+ = 0)\varphi_j(\boldsymbol{r}) \tag{9}$$

where the $\varphi_j$ are the linear combinations of Gaussian orbitals. In our calculations the Gaussian basis set consisted of 13 s, 10 p, five d and one f functions. The lattice constant used was $a = 5.406$ au. As mentioned earlier, the exchange–correlation potential of von Barth and Hedin [32] as parametrized by Rajagopal *et al* [33] was used. Spin–orbit coupling and other relativistic effects were ignored. The SC potential so obtained was used to calculate the band structure and wavefunctions on 506 $\boldsymbol{k}$-points in the 1/48th part of the Brillouin zone (BZ). Using a total of 1409 reciprocal lattice vectors, the EMD, $\rho(\boldsymbol{p})$, contributed by the band electrons was calculated up to $p = 10.0$ au. The EMD thus calculated yielded a value of 7.94 electrons for iron (the ideal theoretical value being 8.00) and this indicated the high accuracy of the present calculations. It may be pointed out that the experimental directional CP [37] and magnetic CP [16] results have been reported up to $p_z = 10.0$ au, and this calls for the theoretical calculation of $\rho(\boldsymbol{p})$ up to at least $p = 10.0$ au.

In the calculation of TPMD we used 135 reciprocal lattice vectors and computed TPMD only up to $p = 4.0$ au because the contribution of the band electrons to TPMD was found to be insignificant beyond $p = 4.0$ au. The 2D ACAR curves, $N(p_y, p_z)$, were calculated by generating TPMD values at more than 40 000 points in the 1/48th volume of $\boldsymbol{p}$-space.

## 3. Results and discussion

### *3.1. Band structure and Fermi surface*

The present results for the band structure and FS topology for the majority- and minority-spin electrons of iron agree very well with those reported by Callaway and Wang [30],

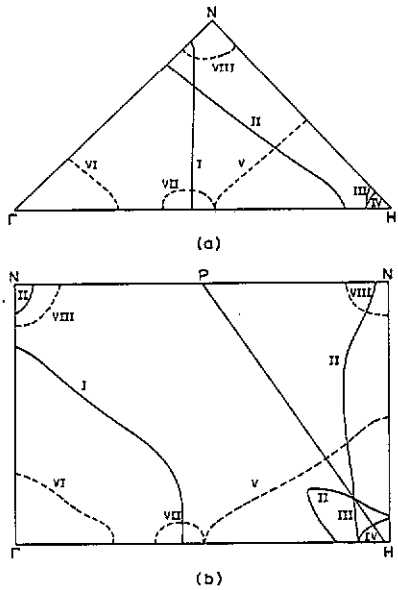


**Figure 1.** Cross sections of the Fermi surface of iron in (*a*) ⟨100⟩ plane and (*b*) ⟨110⟩ plane. Majority-spin sheets are represented by full curves, minority by broken curves. The Roman numerals refer to the assignment given in table VI of [30].

earlier. In view of this, the plots of band structure are not presented here. Instead we show in figures 1(*a*) and (*b*) the present results for the FS topology of iron because we shall discuss our present results for the MD in terms of these topologies. The Roman numerals on the FS sheets in figure 1 refer to the description of the FS as given in table VI of [30].

The value of the magnetic moment per site obtained by us is 2.16 $\mu_B$, which agrees well with the previously reported experimental value of 2.12 $\mu_B$ [38] and theoretical values of 2.16 $\mu_B$ [30] and 2.15 $\mu_B$ [39]. It may be pointed out that the SC band-structure calculations of iron have always resulted in values of magnetic moments that are higher than the experimental value.

### *3.2. Momentum distributions*

Present results for the EMD and TPMD have been obtained by us in three forms: (i) directional curves of $\rho(\boldsymbol{p})$ along different ⟨*hkl*⟩ directions, (ii) perspective plots of the surfaces $\rho(p_x, p_y)$ plotted in various symmetry planes $(p_x, p_y)$, and (iii) contour plots of the surfaces $\rho(p_x, p_y)$ in the $(p_x, p_y)$ planes. However, for want of space we shall present here only some typical plots. More plots can be supplied on request.

The directional curves of $\rho(\boldsymbol{p})$ and $\rho^{2\gamma}(\boldsymbol{p})$ obtained by us and their angular momentum dependence (i.e. on the $l$ state of the band electron) show features similar to those already reported by Mijnarends [18], Kanhere and Singru [40] and Sob [23], and consequently they are not discussed here. Instead, the perspective plot of the EMD, $\rho(\boldsymbol{p})$, in the (100) plane is shown in figure 2 while the contour plot of the EMD, $\rho(\boldsymbol{p})$, in the (110) plane is shown in figure 3, both for the case of majority-spin electrons. The complex topology of the FS of iron is reflected in the shape and structure of these plots. The EMD surface in the (100) plane (figure 2) shows a sharp discontinuity occurring in the region $p < 0.8$ au (first BZ) and this corresponds to the FS sheet I (figure 1) consisting of the large Γ-centred majority-spin electron surface. The Umklapp image of this surface in

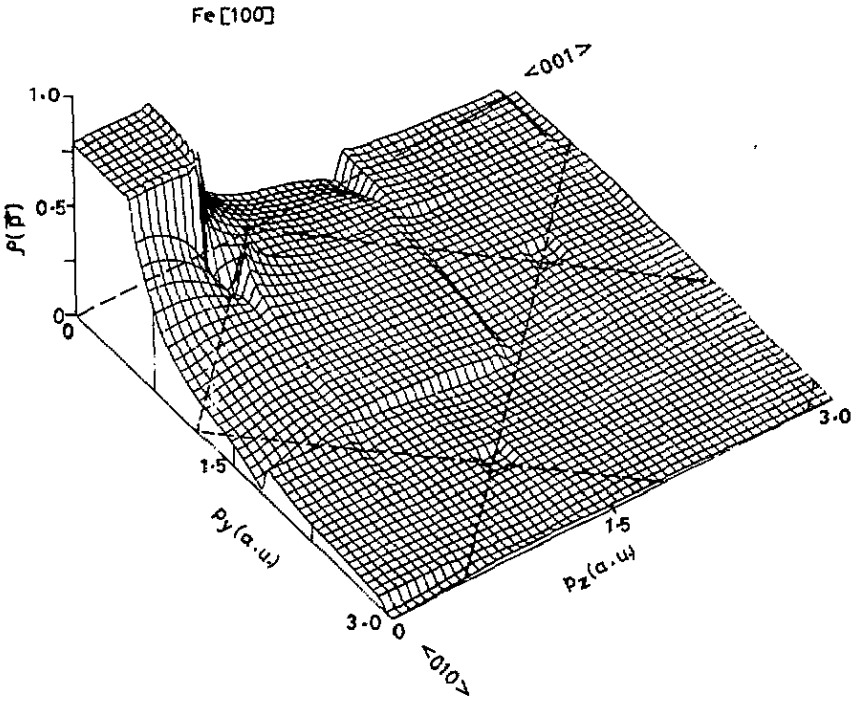


**Figure 2.** Section of the EMD, $\rho(p)$, in iron by the $\langle 100 \rangle$ plane for the majority spin. The broken lines indicate the section of the BZ in the same plane.

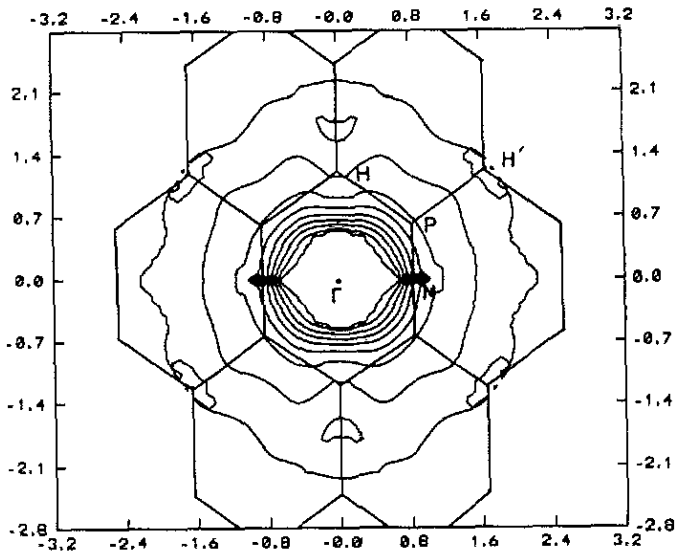


**Figure 3.** Contour plot of the EMD, $\rho(p)$, in iron in the $\langle 1\,1\,0 \rangle$ plane for the majority spin. The interval between neighbouring isodenses is 0.08 units.

the second BZ is seen in figure 2 in the form of a wedge-like structure spread across the second BZ, and it clearly brings out the topology of this surface I. The majority-spin surfaces III and IV (figure 1) are the intermediate and small H-centred hole pockets, respectively, and in the (100) plane they arise out of the $\Delta_2'$ (or $F_3$ or $G_1$) and $\Delta_5$ (or $F_1$ or $G_3$) bands, respectively. These hole pockets do not seem to give rise to any structure in the EMD surface in the first BZ (figure 2). This behaviour can be understood on the basis of the so-called symmetry selection rule [9, 41], according to which certain bands, depending on their group-theoretical representation, are not allowed to contribute to the EMD (or TPMD) along certain directions or planes. Using the tables given in [9] and [41] it is seen that the H-centred intermediate and small hole pockets are prevented from giving rise to discontinuities in the EMD surface in the first BZ of the (100) plane. They can, however, contribute to the EMD in the higher zones and hence their presence is manifested in the form of small depressions around H in the higher zones. Similar analysis involving the directional curves of MD has been given earlier [18, 19, 23].

The contour plot of the EMD for the majority-spin electrons in the (110) plane brings out the topology of the FS sheets in a similar manner. Once again the effect of the Γ-centred surface I (figure 1) is seen prominently inside the I BZ and its Umklapp images are seen weakly in the higher zones. Similarly the effect of the H-centred surfaces III and IV are seen not in the first BZ but in the higher zones around H (e.g. along the ⟨111⟩ direction at $p \sim 2.0$ au).

The perspective plots of the TPMD, $\rho^{2\gamma}(\boldsymbol{p})$, are not shown here but they exhibit [31] features similar to those observed in figures 2 and 3. One important difference observed in the TPMD surfaces is that the higher-zone Umklapp images are smaller in amplitude and hence are barely visible. This difference between the TPMD and EMD is well known and is attributed to the effect of the positron wavefunction. To give a specific example, the H-centred small hole pockets (surfaces III and IV) are not seen clearly in the TPMD surfaces or their contours.

It was pointed out earlier that a certain ambiguity exists in the literature about the FS topology of iron. Most of the differences revolve around two sheets: (i) Majority-spin hole surface II (figure 1)—according to some authors these hole arms linking the points H–N–H are continuous at N, while some authors observe that the arms are pinched at N. (ii) Minority-spin hole pocket around N (sheet VIII in figure 1)—one would like to know whether this hole pocket exists and if so with what size. Examination of the band structure shows that the ordering of levels in the neighbourhood of the point N holds the key to this riddle. Our calculated band structure of iron indicates that the majority-hole arms (sheet II) are not pinched at N and that minority-spin hole pockets of a fair size exist around N [31].

It would be of interest to examine how the study of MD can clear these ambiguities. Mijnarends [18] has discussed this aspect in detail, and after analysing his spin-dependent 1D ACAR data for iron he has concluded that the minority-spin hole pockets are either extremely small in size or are absent. A recent study of this problem was carried out by Genoud *et al* [20], who measured spin-dependent 2D ACAR for ferromagnetic iron and compared it with LMTO theory. These authors came to the conclusion that the possible existence of a small-sized N-centred hole ellipsoid in the FS of minority electrons of iron cannot be ruled out, although the size of this hole pocket is expected to be much smaller than that predicted by various SC band-structure calculations. In a later study of the spin-dependent CP from iron, Genoud and Singh [28] rule out the existence of these hole pockets.

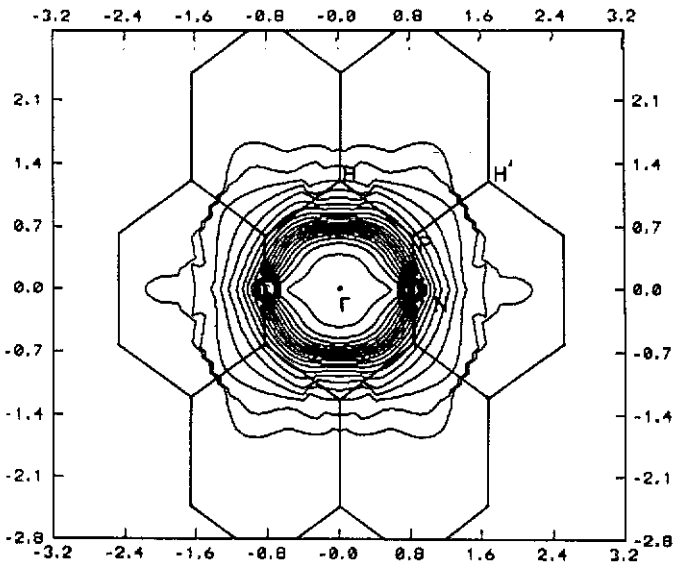


**Figure 4.** Contour plot of the TPMD, $\rho^{2\gamma}(\boldsymbol{p})$, in iron in the ⟨1 1 0⟩ plane for the minority spin. The interval between neighbouring isodenses is 0.05 units.

To illustrate the role played by the TPMD in this ambiguity, we show in figure 4 the contour plot of TPMD contributed by minority electrons in the (1 1 0) plane. This plot offers an idea about the size and shape of structure around the point N. In our opinion this structure is just above the limit that can render it observable in the reconstructed TPMD plots. Previous attempts at reconstruction of TPMD in Ti [42], V [43], Cu [44], Zn [45], Zr [42] and Gd [46] have already shown that it is possible to reconstruct the TPMD, $\rho^{2\gamma}(\boldsymbol{p})$, from the measured sets of 2D ACAR surfaces and that such an exercise can help us to distinguish between different models of band structure and FS. We propose that such a reconstruction of the spin-dependent TPMD in ferromagnetic iron should be undertaken to resolve the ambiguity around the point N. Although such a comprehensive reconstruction of the EMD, $\rho(\boldsymbol{p})$, from the measured CP data appears to be a difficult proposition [7], the picture is definitely going to change in the near future in view of the promising developments in measuring the CP with higher momentum resolution and better efficiency by using synchrotron radiation [47]. Analysis of the EMD and TPMD in terms of the FS topology as given above will prove useful for interpreting reconstructed MD for iron. Present calculations have resulted in a rich collection of data in terms of surfaces, line and contour plots of EMD, TPMD, CP and ACAR for iron. These results, although not presented here, can be made available on request.

In order to bring out the angular momentum dependence of the EMD and TPMD in iron, we have shown in table 1 a comparison of the weighted areas under the pure s-, p- and d-wave contributions to the momentum distributions along the ⟨1 0 0⟩, ⟨1 1 0⟩ and ⟨1 1 1⟩ directions for the majority- and minority-spin electrons. The results in table 1 indicate the substantial d-wave contribution to the MD because the d components are dominant beyond $p = 1.0$ au, which increases their weighted area relative to that of the s and p components. It is also seen that the percentages of s and p contributions are higher in the TPMD than in the EMD. This behaviour is attributed to the effect of positron wavefunction. One also observes from table 1 that (i) the angular momentum

**Table 1.** The ratio of the weighted areas of *pure* s, p and d contributions[a] to the total momentum distributions in iron.

| | s | | p | | d | |
|---|---|---|---|---|---|---|
| Direction | EMD | TPMD | EMD | TPMD | EMD | TPMD |
| Majority spin | | | | | | |
| ⟨100⟩ | 0.047 | 0.093 | 0.044 | 0.088 | 0.882 | 0.709 |
| ⟨110⟩ | 0.073 | 0.163 | 0.062 | 0.136 | 0.815 | 0.574 |
| ⟨111⟩ | 0.032 | 0.079 | 0.047 | 0.095 | 0.760 | 0.531 |
| Minority spin | | | | | | |
| ⟨100⟩ | 0.099 | 0.118 | 0.150 | 0.201 | 0.690 | 0.494 |
| ⟨110⟩ | 0.088 | 0.177 | 0.084 | 0.175 | 0.776 | 0.528 |
| ⟨111⟩ | 0.044 | 0.092 | 0.093 | 0.164 | 0.597 | 0.333 |

[a] The sum of s, p and d contributions along any direction does not add up to 1.000 because the hybridized part is not taken into account.

dependence of both the MD is highly anisotropic and (ii) the percentage contribution of a particular $l$ state is different for the two spins, the percentage of the s and p contributions being higher for the minority-spin electrons. In this connection it should be pointed out that Genoud *et al* [20] had to use different enhancement factors, $\varepsilon(\gamma)$, for the majority- and minority-spin electrons to correct for the $e^+$–$e^-$ many-body correlations before their LMTO theory could describe the 2D ACAR data accurately.

We have defined the spin momentum density (SMD), $\Delta\rho(\boldsymbol{p})$, as

$$\Delta\rho(\boldsymbol{p}) = \rho_{\mathrm{maj}}(\boldsymbol{p}) - \rho_{\mathrm{min}}(\boldsymbol{p}) \tag{10}$$

and have shown its contour plot in the (100) plane in figure 5. It is observed that the SMD in iron exhibits considerable anisotropy and structure, which are larger compared to those in ferromagnetic nickel [31]. These differences are attributed to the different topologies of the FS in these two metals. Close examination of the results of figure 5 shows negative SMD around the point N arising from the minority hole pocket centred around N. It is suggested that a reconstruction of the SMD for ferromagnetic iron should be attempted so that experimental results can be compared with those in figure 5, with the aim to verify the presence of the N-centred minority hole pocket.

### *3.3. Compton profile*

Several measurements of the non-magnetic [37] and magnetic [12–16] CP of iron have been reported in the literature, and we present in the following subsections a comparison of our theoretical CP with experiment.

*3.3.1. Non-magnetic Compton profile.* Rollason *et al* [37] have measured the directional non-magnetic CP from single crystals of iron using 412 keV gamma radiation from $^{198}$Au. These authors have compared their experimental results with the theoretical results obtained by the APW [22] and LCGO [26] methods. As pointed out earlier, the present computation had the advantages of calculating the EMD up to $q = 10.0$ au (as compared to the APW method [22], which calculated the EMD up to $q = 5.0$ au only) and of including the von Barth–Hedin exchange–correlation potential (as compared to the previous LCGO

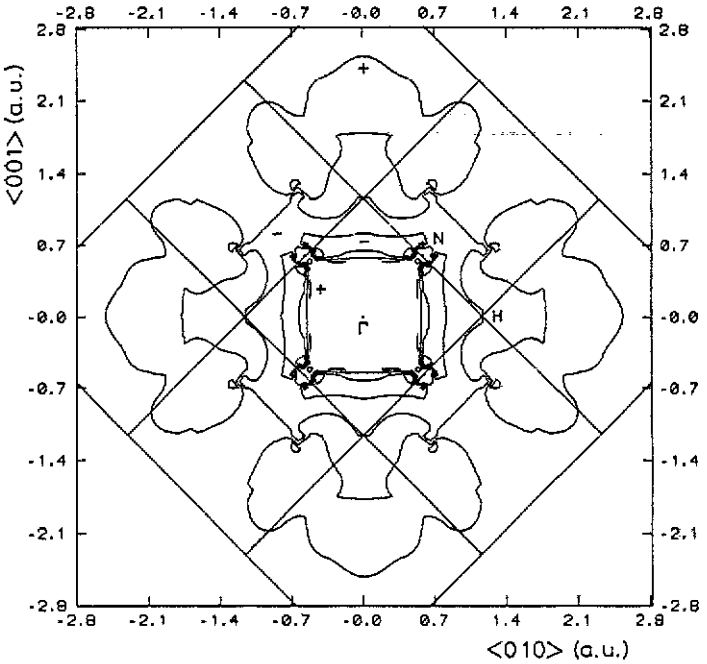


**Figure 5.** Contour plot of the SMD, $\Delta\rho(p)$, in the $\langle 100 \rangle$ plane. The interval between neighbouring isodenses is 0.08 units. The regions marked '+' have dominant contribution from the majority-spin, while those marked '−' have dominant contribution from the minority-spin electrons.

calculation [26], which used an exchange-only potential). The 'missing' electron part was only 0.03 electrons/spin in the present calculation. In view of these advantages a comparison of the experiment with the present theory should provide some new information besides offering a test of the quality of wavefunctions used. To determine the theoretical non-magnetic CP, the contributions from the majority- and minority-spin electrons were first added up and the resulting profiles were then convoluted with a Gaussian of FWHM = 0.4 au before comparing them with experiment [37]. Such a comparison of the difference ($(J_{111} - J_{100})$, etc) profiles is shown in figure 6. The inclusion of the exchange–correlation appears to have improved the agreement between theory and experiment. For example, the crossings near 1.9 au for (111 − 100) and near 2.4 au for (111 − 110) now match better. Similarly the oscillatory behaviour in the difference profiles for $p_z > 2.0$ au is now reproduced by the theory quite well. However, the size of the differences at $p_z = 0$ is now overestimated compared to the previous work except in the case of (110 − 100). This might be due to the difference in the two normalizations, among other reasons. On the whole it can be said that the inclusion of correlations generally improves the anisotropies of the CP curves. We also observe, in agreement with the previous report [37], that the anisotropies in iron are much smaller than those observed in other transition metals (e.g. V, Cr, Cu, etc) and that the structure observed in the difference profiles (figure 6) cannot be easily correlated with the important features of the FS of iron.

It was pointed out by Bauer and Schneider [48] that the discrepancies between the peak heights of the experimental and theoretical difference CP in metals (such as those

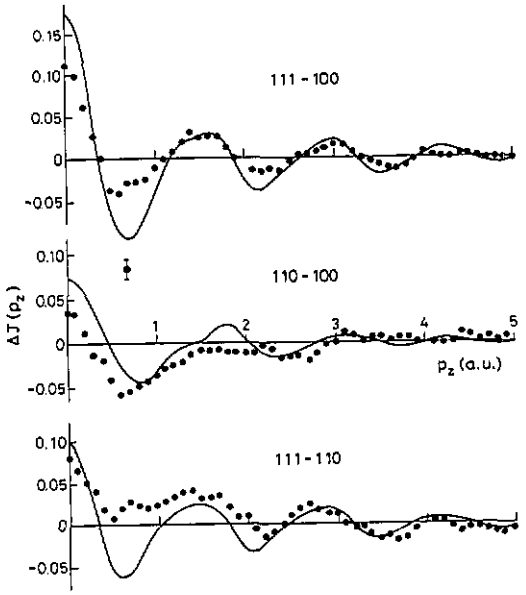


**Figure 6.** Difference Compton profiles $\Delta J(p_z)$ in iron for three pairs of directions. The full circles represent the experimental data [37] while the full curves represent the present theory after convoluting it with a Gaussian of FWHM = 0.4 au.

in figure 6) could be attributed to the neglect of electron–electron correlations in the band models used. To test this, we applied the so-called Lam–Platzman correction [49] to the present theoretical results for the CP. Such a procedure brought down the differences between theoretical and experimental directional CP from 0.8 to 0.3 electrons/au for the ⟨100⟩ direction, from 0.12 to 0.06 electrons/au for the ⟨110⟩ direction and from 0.14 to 0.09 electrons/au for the ⟨111⟩ direction. Although this trend is in the right direction, the theory still overestimated the profiles in the region $q < 2.0$ au. The effects also appear to be anisotropic, while the Lam–Platzman correction is isotropic in nature. A solution to this problem in the case of chromium has been suggested recently by Cardwell *et al* [50], who have calculated anisotropic correlation effects in CP using the three-dimensional APW density of states. We feel that a similar approach for treating electron–electron correlations and non-locality is needed for ferromagnetic iron.

*3.3.2. Magnetic Compton profile.* As mentioned in section 1, several workers have measured spin-dependent Compton scattering from iron to study the MD of electrons involved in its ferromagnetism. Collins *et al* [16] have reported the directional magnetic Compton profiles measured along the ⟨100⟩, ⟨110⟩ and ⟨111⟩ directions. Figure 7 shows a comparison between their experiment and present theory. The theoretical profiles have been convoluted with a Gaussian of FWHM = 0.7 au and normalized appropriately. Although all the three theoretical magnetic CP in figure 7 show a central dip (for $p_z < 1$ au) in agreement with experiment [16] and APW [51], KKR [25], previous LCGO [26] and LMTO [28] theories, the sizes of the central dip are not predicted accurately by any of these theories. There is good agreement between different theories and between experiment and theory in the region $p_z > 2$ au. Although different theories agree among them in the low-momentum region ($p_z < 2$ au), they all disagree with the experiment for the ⟨110⟩

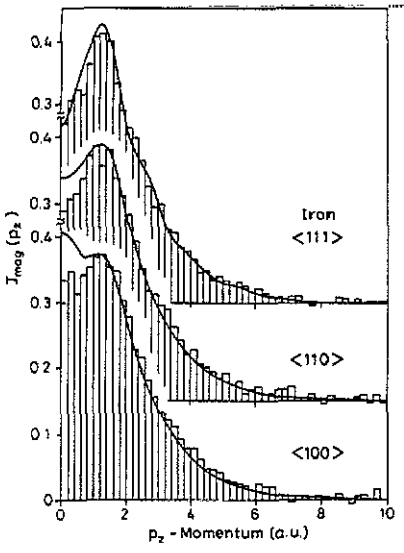


**Figure 7.** Directional magnetic Compton profile in iron along the ⟨100⟩, ⟨110⟩ and ⟨111⟩ directions. The histograms represent the experimental data [16] while the full curves represent the present theory after convoluting it with a Gaussian of FWHM = 0.7 au.

and ⟨100⟩ profiles, with the latter CP exhibiting the largest discrepancy. Using a parametrized LMTO method, which gave vanishing size for the N-centred hole pocket of the minority third band, Genoud and Singh [28] have observed that the theoretical magnetic CP can be brought very close to the experimental curves for the [111] and [110] directions, but the theory still overestimated the magnetic CP for the [100] direction near $p_z = 0$. This behaviour has been attributed to the inadequate estimation of the negatively polarized 4s–p band in their theory [28]. The comparisons presented in figure 7 and elsewhere [16, 28] clearly show that the differences between experiment and theory are not due to the artifacts of different band theories and that they cannot be completely removed by a parametrized calculation. We feel that these differences arise out of the inadequacy of the representation of the FS topology and electron–electron correlation effects. A more *ab initio* theoretical approach, free of any parameters, is perhaps needed to solve this problem. On the experimental side this challenging problem can be solved by measuring the magnetic CP with better momentum resolution and higher statistical accuracy, as planned by the group at the Photon Factory, Ibaraki, Japan [47].

It may be mentioned that we have also calculated the majority- and minority-band directional difference profiles using equations (7)–(10) of [16] and compared them with experiment [16]. The trend of the present theoretical results is close to that predicted by the APW theory [51].

### *3.4. Positron annihilation (ACAR)*

*3.4.1. Introduction.* The ACAR technique has two important experimental advantages: (i) high momentum resolution and (ii) choice of 1D or 2D geometry. On the theoretical side, the interpretation of the results is complicated by the positron wavefunction and $e^+$–$e^-$ many-body correlation effects. However, considerable progress has been made in calculating these effects and incorporating them in the IPM theory [8–11]. With its added capability of measuring spin-dependent TPMD, the ACAR technique is a powerful tool to study the FS of ferromagnetic metals. We shall now present our theoretical results for ACAR and shall compare them with experiment wherever possible.

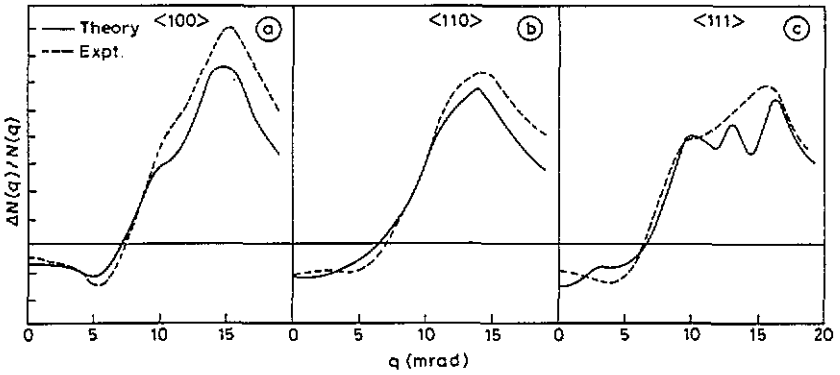


**Figure 8.** Magnetic 1D ACAR curves in iron. See equations (11) and (12) for the definition of $N(q)$ and $\Delta N(q)$. The full curves indicate the present calculations while the broken curves denote the experimental data [18].

*3.4.2. One-dimensional ACAR.* In this section we shall present a comparison of our theoretical ACAR results with those measured by Mijnarends [18] using 1D geometry. Following Wakoh and Kubo [22] we have constructed the magnetic profiles (or the difference curves) $\Delta N(q)/N(q)$, where $N(q)$ denotes the 1D ACAR curve, obtained from

$$N(q) = N_{\mathrm{maj}}(q) + N_{\mathrm{min}}(q) \tag{11}$$

and

$$\Delta N(q) = N_{\mathrm{maj}}(q) - N_{\mathrm{min}}(q). \tag{12}$$

The present theoretical $\Delta N(q)/N(q)$ curves are compared with the experimental results [18] for the three directions $\langle 1\,0\,0\rangle$, $\langle 1\,1\,0\rangle$ and $\langle 1\,1\,1\rangle$ in figure 8. It is observed that the agreement between experiment and present theory is good except in the region $q > 10.0$ mrad (1 mrad $= 10^{-3} m_0 c \simeq 7.29$ au). Additional structure is observed in the present theoretical curve along the $\langle 1\,1\,1\rangle$ direction. Similar behaviour was observed for the APW theory [22]. Two important points have to be kept in mind while analysing the comparison shown in figure 8. First, the present theory did not include the $e^+$–$e^-$ many-body correlations; and secondly, some uncertainty exists in the vertical scale of the experimental $\Delta N(q)/N(q)$ curves brought in by the so-called $P_{3\gamma}$ process [8, 17]. Nevertheless these results (figure 8) assure that the present LCGO theory provides a good basis to describe the TPMD in iron. Having confirmed this, we shall now present our results for the 2D ACAR in iron.

*3.4.3. Two-dimensional ACAR.* We have calculated several 2D ACAR surfaces $N(p_y, p_z)$ for the majority- and minority-spin electrons using equation (7). These surfaces (not presented here) show some structure, which can be interpreted in terms of FS topology in a manner similar to the analysis reported for paramagnetic Cr [52]. We could not compare these theoretical 2D ACAR surfaces with experiment [20] because the experimental data sets $N(p_y, p_z)$ were not available. It has been shown recently [53] that the $e^+$–$e^-$ many-body correlation corrections are $l$-dependent in nature, and their treatment requires a careful fitting with experiment. In the absence of experimental data sets, we could not attempt such an analysis. Instead, we have presented in figures 9–11 our theoretical results in the form of plots obtained by applying the LCW theorem [36] to the

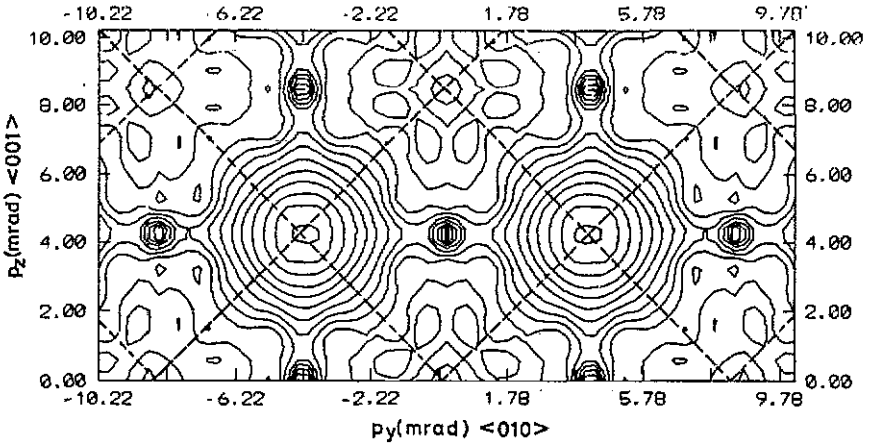


**Figure 9.** LCW-folded 2D ACAR distributions for the majority-spin electrons in iron. Integration axis is along the ⟨100⟩ direction. In these calculations the TPMD, $\rho^{2\gamma}(p)$, was obtained by adding the contribution of band electrons to 0.2 times the contribution from the core electrons.

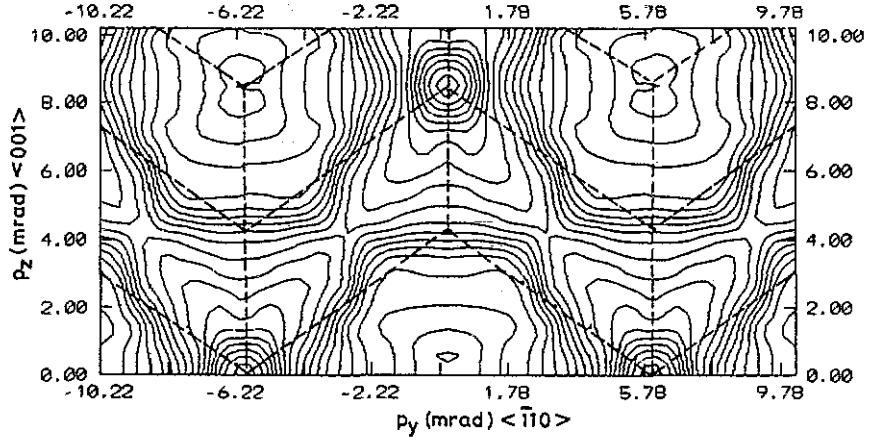


**Figure 10.** Same as in figure 9 but with the integration axis along the ⟨1 1 0⟩ direction.

2D ACAR results. It has been shown [54] that, in spite of the limited validity of the LCW theorem for positron annihilation, the LCW plots provide an important and useful visual mode for comparing theory with experiment. Keeping this in mind, we have shown in figures 9 and 10 the contours of the LCW-folded 2D ACAR distributions in iron for the majority spin with the integration axis along the ⟨1 0 0⟩ and ⟨1 1 0⟩ directions, respectively. The effects of the FS topology (the sheets I, II, III and IV of figure 1) are clearly observed in figures 9 and 10. To carry out the LCW analysis in some detail we have shown in figure 11 the LCW plot along some important symmetry lines of the BZ. The theoretical contributions to the 2D ACAR by the majority- and minority-spin electrons were first added up and then convoluted with the experimental resolution ($0.3 \times 0.5$ mrad$^2$) used by Genoud *et al* [20] before obtaining the plot shown in figure 11. When compared with

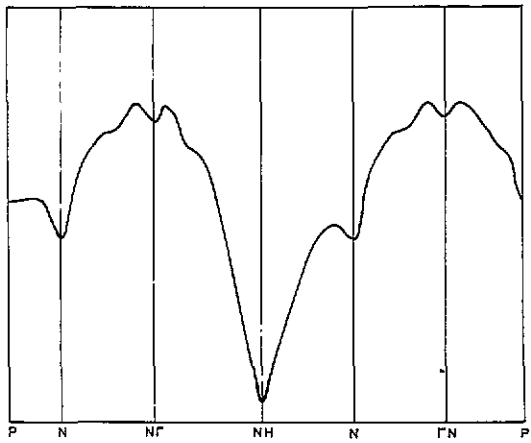


**Figure 11.** LCW analysis of the 2D ACAR distributions along some important symmetry lines of the BZ. The TPMD was obtained by adding the contribution of band electrons to 0.2 times the contribution from the core electrons.

the LMTO theory the present LCW plot (figure 11) shows good agreement. It also agrees well with the experiment [20], although some differences do exist. Most of these major differences occur around the point $N$ and these are attributed to the differences in the FS topology around $N$. The residual differences are minor and they can be ascribed to the neglect of $e^+$–$e^-$ many-body correlation in the present theory.

### *3.5. Autocorrelation function B(z)*

The autocorrelation function (or the reciprocal form factor) $B(z)$ derived from the CP [7, 55] and ACAR [8] data enables us to analyse the results of MD in yet another way. One can define [8]

$$B^{CP}(z) = (2\pi)^{-1/2} FT_{-1}(J(p_z)) \tag{13}$$

and

$$B^{2\gamma}(z) = (2\pi)^{-1/2} FT_{-1}(N(p_z)) \tag{14}$$

where $J(p_z)$ and $N(p_z)$ are Compton profiles and 1D ACAR curves respectively and $FT_{-1}$ denotes the Fourier transform. Recent analysis of these autocorrelation functions in V [56], Cr [31], Ni [31], Cu [31] and Nb [57] have already provided interesting information.

We have calculated the present theoretical $B^{CP}(z)$ and $B^{2\gamma}(z)$ functions in Fe along the ⟨100⟩, ⟨110⟩ and ⟨111⟩ directions after (i) summing the contributions from the majority- and minority-spin electrons, (ii) taking into account the effect of finite resolution and (iii) normalizing the curves to 26 electrons at $z = 0$. Although these curves have not been presented here, the trend of the present theoretical curves has been observed by us to be similar to the APW [22] and the earlier LCGO [26] theoretical results as reported by Rollason *et al* [37]. We have also compared the experimental results for the $B^{CP}(z)$ curves [37] with our theory and have observed that the inclusion of the correlation effects has brought the present theoretical $B^{CP}(z)$ curves closer to the experiment. Some differences between the theory and experiment still persist, and this

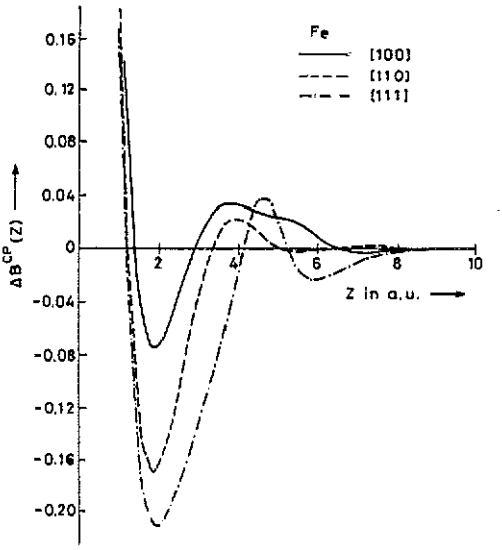


**Figure 12.** The difference curve $\Delta B^{CP}(z)$ defined by equation (15) along the [100] (——), [110] (– – –) and [111] (– · – · –) directions.

behaviour indicates that the electronic wavefunctions need further improved theoretical description, particularly along the ⟨111⟩ direction, which is the direction of nearest neighbours.

We have also compared the theoretical $B^{CP}(z)$ and $B^{2\gamma}(z)$ curves because both these are calculated using the same set of electron wavefunctions. Two prominent features emerge out of such a comparison. First, the $B^{2\gamma}(z)$ curves show high amplitudes at large $z$ values ($z > 10.0$ au) while the $B^{CP}(z)$ curves damp out in this region. Secondly, the $B^{2\gamma}(z)$ curves are smoother in comparison to the corresponding $B^{CP}(z)$ curves in the region $z = 3.0$ to 10.0 au. Similar behaviour has been observed in the case of V and has been attributed to the effect of positron wavefunction [56].

The spin-dependent anisotropy of the autocorrelation function $B(z)$ has not been reported in the literature so far. Keeping this in mind, we have used the present theoretical $B(z)$ curves for the majority- and minority-spin electrons of Fe to define the difference curves $\Delta B^{CP}(z)$ for Compton profiles and $\Delta B^{2\gamma}(z)$ for positron annihilation, through the equation

$$\Delta B(z) = B_{maj}(z) - B_{min}(z). \tag{15}$$

The difference curves $\Delta B^{CP}(z)$ and $\Delta B^{2\gamma}(z)$ obtained from the present theory are shown in figures 12 and 13 respectively for three crystalline directions in Fe. These results show that the spin autocorrelation function is anisotropic in $r$-space with the ⟨111⟩ direction (i.e. the direction of nearest neighbours) showing the largest amplitude in the region $z = 2.0$ to 4.0 au. It has been shown [58] that the autocorrelation function $B(r)$ is sensitive to the $e_g : t_{2g}$ electron population ratios in the transition metals. The behaviour of the results shown in figures 12 and 13 can be understood in terms of the spatial behaviour of the electron wavefunctions and the different $e_g : t_{2g}$ ratios in the two spin states of iron. A comparison of the radial dependence of $\Delta B^{CP}(z)$ and $\Delta B^{2\gamma}(z)$ (figures 12 and 13) also brings out the effects of positron wavefunction of the spin autocorrelation

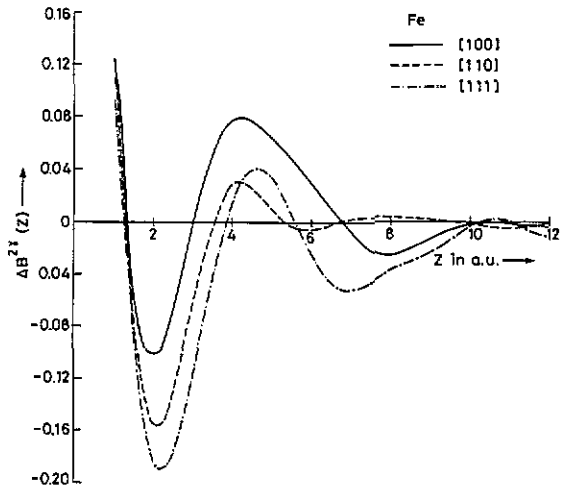


**Figure 13.** Same as in figure 12 but for $\Delta B^{2\gamma}(z)$.

function. In view of all this, it should be interesting to analyse future experimental measurements of the spin-dependent CP and ACAR curves in Fe in terms of $\Delta B^{CP}(z)$ and $\Delta B^{2\gamma}(z)$, with the present results providing a theoretical basis.

## 4. Summary and conclusions

The EMD, $\rho(\boldsymbol{p})$, and the TPMD, $\rho^{2\gamma}(\boldsymbol{p})$, in ferromagnetic iron have been calculated with the LCGO method (containing better treatment of exchange–correlation) using the same set of electron wavefunctions. Various observable physical quantities have been computed and these theoretical results are compared with experiment wherever possible. The effects of FS topology are pointed out and comments are made about the design and data analysis of CP and 2D ACAR experiments with a view to resolving the ambiguities about the FS topology.

It is concluded that the LCGO method, in the independent-particle model (IPM), provides a satisfactory description of the gross features of the measured momentum distributions. On a finer scale, several discrepancies between theory and experiment were found. These discrepancies were present even when other IPM theoretical calculations (like the APW method, LMTO theory) were used for comparison by other workers. Hence it appears that there is some inadequacy present in all IPM calculations. Although a parametrized LMTO calculation improves the fit with experiment, this appears as an *ad hoc* solution of the problem. It is certain that the theoretical description of the band structure, FS, $e^-$–$e^-$ and $e^+$–$e^-$ many-body correlations in ferromagnetic iron needs further improvement by using a more *ab initio* approach.

## Acknowledgments

The authors wish to thank Dr M J Cooper, Dr N Shiotani and Dr A K Singh for communicating their results prior to publication. Financial support for this work from

the Department of Science and Technology, Government of India, under their Grant No SP/S2/M-39/87, and the Centre for Development of Advanced Computing, Pune, is gratefully acknowledged.

## References

[1] Lonzarich G G 1980 *Electrons at the Fermi Surface* ed M Springford (Cambridge: Cambridge University Press) ch 6
[2] Nautiyal T and Auluck S 1985 *Phys. Rev.* B **32** 6424
[3] Baraff D R 1973 *Phys. Rev.* B **8** 3439
[4] Gold A V, Hodges L, Panausis P T and Stone D R 1971 *Int. J. Magn.* **2** 357
[5] Coleman R V, Morris R C and Stellmeyer D J 1973 *Phys. Rev.* B **8** 317
Coleman R V, Lowrey W H and Polo J A 1981 *Phys. Rev.* B **23** 2491
[6] Angadi M M, Fawcett E and Rasolt M 1974 *Phys. Rev. Lett.* **32** 613
[7] Cooper M 1985 *Rep. Prog. Phys.* **48** 415
[8] Berko S 1983 *Positron Solid State Physics* ed W Brandt and A Dupasquier (Amsterdam: North-Holland) p 64
[9] Mijnarends P E 1983 *Positron Solid State Physics* ed W Brandt and A Dupasquier (Amsterdam: North-Holland) p 146
[10] Jain P C, Singru R M and Gopinathan K P (ed) 1985 *Positron Annihilation* (Singapore: World Scientific)
[11] Dorikens-van Praet L, Dorikens M and Segers S (ed) 1989 *Positron Annihilation* (Singapore: World Scientific)
[12] Cooper M J, Laundy D, Cardwell D A, Timms D N, Holt R S and Clark G 1986 *Phys. Rev.* B **34** 5984
[13] Sakai N and Sekizawa H 1987 *Phys. Rev.* B **36** 2164
[14] Mills D M 1987 *Phys. Rev.* B **36** 6178
[15] Timms D N, Brahmia A, Collins S P, Cooper M J, Holt R S, Kane P P, Clark G and Laundy D 1988 *J. Phys. F: Met. Phys.* **18** L57
[16] Collins S P, Cooper M J, Timms D, Brahmia A, Laundy D and Kane P P 1989 *J. Phys.: Condens. Matter* **1** 9009
[17] Berko S and Zuckerman J 1964 *Phys. Rev. Lett.* **13** 339
Berko S and Mills A P 1971 *J. Physique* **23** (C1) 287
[18] Mijnarends P E 1973 *Physica* **63** 235, 248
[19] Szuszkiewicz S, Rozenfeld B and Szuszkiewicz M 1979 *Phys. Status Solidi* b **94** 273
[20] Genoud P, Singh A K, Manuel A A, Jarlborg T, Walker E, Peter M and Weller M 1988 *J. Phys. F: Met. Phys.* **18** 1933
[21] Wakoh S, Kubo Y and Yamashita J 1975 *J. Phys. Soc. Japan* **38** 416
Wakoh S, Fukamachi T, Hosoya S and Yamashita J 1975 *J. Phys. Soc. Japan* **38** 1601
Wakoh S, Kubo Y and Yamashita J 1976 *J. Phys. Soc. Japan* **40** 1043
[22] Wakoh S and Kubo Y 1977 *J. Magn. Magn. Mater.* **5** 202
[23] Sob M 1982 *J. Phys. F: Met. Phys.* **12** 571
[24] Wakoh S and Yamashita J 1973 *J. Phys. Soc. Japan* **35** 1406
[25] Poulter J and Staunton J B 1988 *J. Phys. F: Met. Phys.* **18** 1877
[26] Rath J, Wang C S, Tawil R A and Callaway J 1973 *Phys. Rev.* B **8** 5139
[27] Jansen H J F and Muller F M 1982 *Phys. Rev.* B **26** 2624
[28] Genoud P and Singh A K 1989 *J. Phys.: Condens. Matter* **1** 5363
[29] Wang C S and Callaway J 1978 *Comput. Phys. Commun.* **14** 327
[30] Callaway J and Wang C S 1977 *Phys. Rev.* B **16** 2095
[31] Sundararajan V 1988 *PhD Thesis* Anna University, Madras (unpublished)
[32] Von Barth U and Hedin L 1972 *J. Phys. C: Solid State Phys.* **5** 1629
[33] Rajagopal A K, Singhal S P and Kimball J (unpublished) as quoted by Rajagopal A K 1979 *Advances in Chemistry and Physics* ed G I Prigogine and S A Rice (New York: Wiley) vol 41, p 59
[34] Sundararajan V, Kanhere D G and Callaway J 1988 *Phys. Lett.* A **133** 521
[35] Sundararajan V and Kanhere D G 1990 *Pramana J. Phys.* **34** 33
[36] Lock D G, Crisp V H C and West R N 1973 *J. Phys. F: Met. Phys.* **3** 561
Lock D G and West R N 1975 *Appl. Phys.* **6** 249
Beardsley G M, Berko S, Mader J J and Schulman M A 1975 *Appl. Phys.* **5** 375

[37] Rollason A J, Holt R S and Cooper M J 1983 *J. Phys. F: Met. Phys.* **13** 1807
[38] Danan H, Herr A and Meyer A J P 1968 *J. Appl. Phys.* **39** 669
[39] Moruzzi V L, Janak J F and Williams A R 1978 *Calculated Electron Properties of Metals* (Oxford: Pergamon)
[40] Kanhere D G and Singru R M 1977 *J. Phys. F: Met. Phys.* **7** 2603
[41] Harthoorn R and Mijnarends P E 1978 *J. Phys. F: Met. Phys.* **8** 1147
[42] Suzuki R, Osawa M, Tanigawa S, Matsumoto M and Shiotani N 1989 *J. Phys. Soc. Japan* **58** 3251
[43] Pecora L M, Ehrlich A C, Manuel A A, Singh A K, Peter M and Singru R M 1988 *Phys. Rev.* B **37** 6772
[44] Sinclair F, Farmer W S and Berko S 1982 *Positron Annihilation* ed P G Coleman, S C Sharma and L M Diana (Amsterdam: North-Holland) p 322
[45] Daniuk S, Kontrym-Sznajd G, Rubaszek A, Stachowiak H, Mayers J, Walters P A and West R N 1987 *J. Phys. F: Met. Phys.* **17** 1365
[46] Hoffmann K R, Berko S and Beaudry B J 1982 *Positron Annihilation* ed P G Coleman, S C Sharma and L M Diana (Amsterdam: North-Holland) p 325
Waspe R L and West R N 1982 *ibid* p 328
[47] Sakai N, Shiotani N, Ito M, Itoh F, Kawata H, Amemiya Y, Ando M, Yamamoto S and Kitamura H 1989 *Rev. Sci. Instrum.* **60** 1666
Itoh F, Sakurai M, Sugawa T, Suzuki K, Sakai N, Ito M, Mao O, Shiotani N, Tanaka Y, Sakurai Y, Nanao S, Kawata H, Amemiya Y and Ando M 1989 *Rev. Sci. Instrum.* **60** 2402
[48] Bauer G E W and Schneider J R 1985 *Phys. Rev.* B **31** 681
[49] Lam L and Platzman P 1974 *Phys. Rev.* B **9** 5122
[50] Cardwell D A, Cooper M J and Wakoh S 1989 *J. Phys.: Condens. Matter* **1** 541
[51] Wakoh S, quoted by Collins *et al* [16]
[52] Singh A K and Singru R M 1983 *J. Phys. F: Met. Phys.* **13** 2189
[53] Singh A K, Manuel A A, Jarlborg T, Mathys Y, Walker E and Peter M 1986 *Helv. Phys. Acta* **59** 410
[54] Singh A K and Singru R M 1984 *J. Phys. F: Met. Phys.* **14** 1751
Rabou L P L M and Mijnarends P E 1984 *Solid State Commun.* **52** 933
[55] Schülke W 1977 *Phys. Status Solidi* b **82** 229
[56] Singh A K, Manuel A A, Singru R M and Peter M 1985 *Helv. Phys. Acta* **58** 640
[57] Singh A K, Manuel A A, Singru R M, Jarlborg T, Vanuzzio A and Peter M 1985 *Positron Annihilation* ed P C Jain, R M Singru and Gopinathan K P (Singapore: World Scientific) p 273
[58] Mishra R R and Singru R M 1986 *Chem. Scr.* **26** 501